Supplementary Information

Effect of Externally Applied Pressure on Rechargeable Alkaline Zinc Batteries at Limited Depth of Discharge

Deepak Kharel[1], Calvin D. Quilty[2], Igor I. Bezsonov[2], Ciara N. Wright[2], Timothy N. Lambert[2,3], and Yang-Tse Cheng[1,4]**

[1]Department of Physics and Astronomy, University of Kentucky, Lexington, KY 40506, USA

[2]Department of Photovoltaic and Materials Technology, Sandia National Laboratories, Albuquerque, NM 87185, USA

[3]Center for Integrated Nanotechnologies, Sandia National Laboratories, NM 87123, USA

[4]Department of Chemical and Materials Engineering, University of Kentucky, Lexington, KY 40506, USA

*tnlambe@sandia.gov; yang.t.cheng@uky.edu

Electrochemical performance of cell

Electrochemical cycling was performed using a Biologic VMP3 battery cycler. All cells received an initial formation cycle where they were discharged to the desired DOD_{MnO_2}(voltage limit = 0.9 V) at C/20 (based on a theoretical 2 e.e. MnO_2 capacity of 617 mAh g^{-1}) and then charged at C/20 to 1.65 V at which point the voltage was held until the current dropped to 10% of its initial value. Cycling was then performed using the same protocol but at a C/5 rate (based on a theoretical 2 e.e. MnO_2 capacity of 617 mAh g^{-1}).

We conducted replicate experiments across three identical cells under the influence of externally applied pressure to ensure reproducibility in our findings. The electrochemical performance of three identical cells cycled under same protocol and pressure are shown in **Figure S1**. Each of these cells cycled under 2.12 MPa pressure using an in-house built pressure cell. **Figure S2** shows the average voltage-capacity profiles of same selected cycles from three identical cells with error bar representing the standard deviation. The results are consistent and reproducible, and the error bars are within 5% as shown in **Figure S2**.

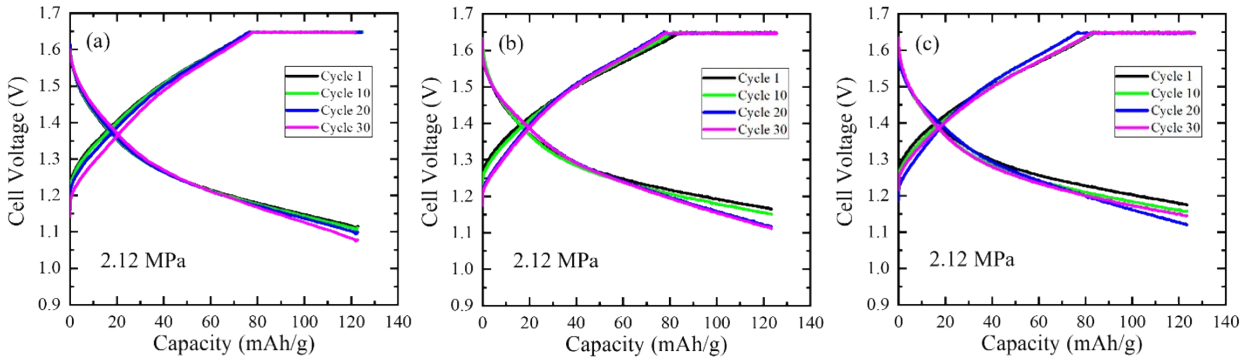

Figure S1: The electrochemical performance of alkaline Zn-MnO_2 batteries cycled at 2.12 MPa. Voltage-capacity profiles of three identical alkaline Zn-MnO_2 cells cycled at 2.12 MPa (a) Cell 1, (b) Cell 2, and (c) Cell 3.

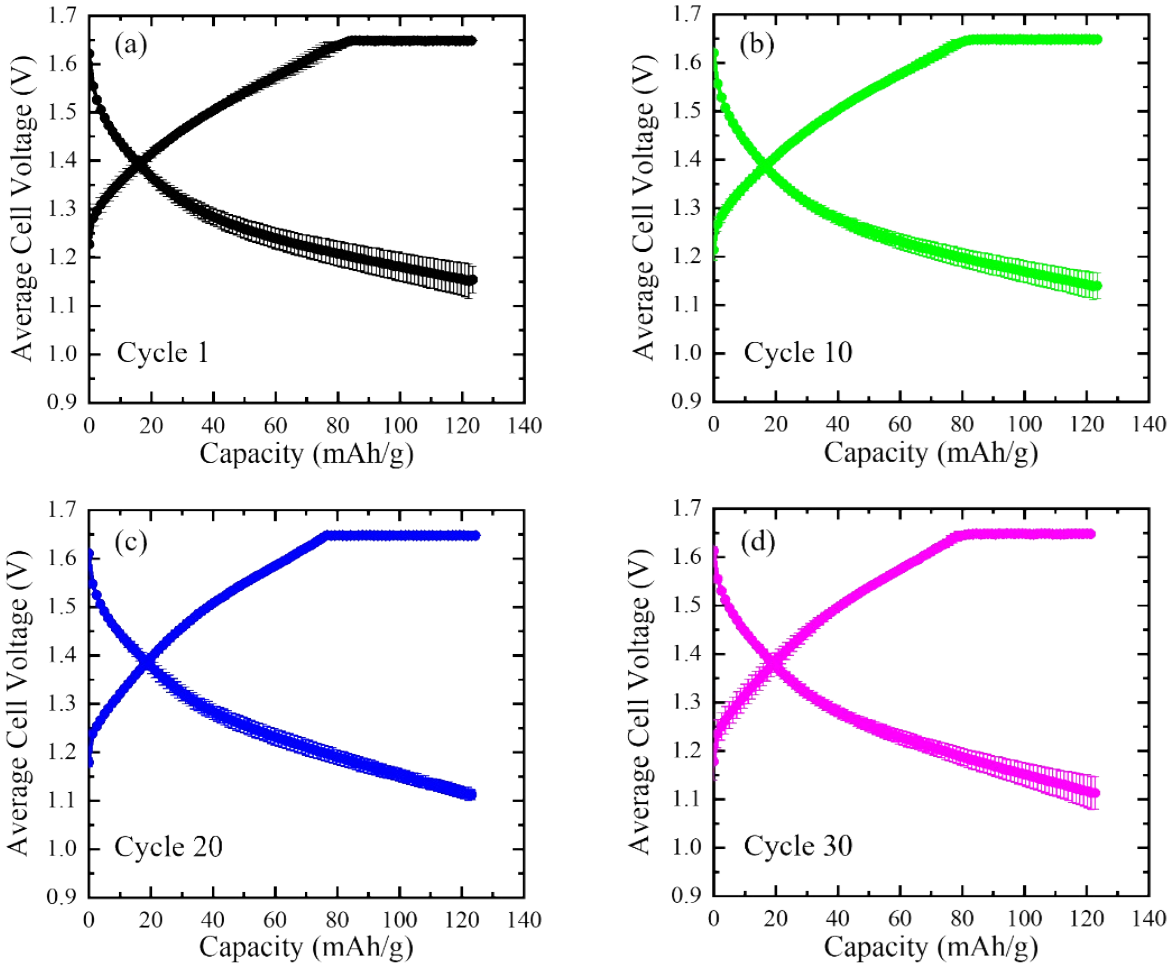

Figure S2: Average voltage-capacity profiles of three identical alkaline Zn-MnO_2 cells cycled at 2.12 MPa. Data represents average of selected cycles from three identical cells, and the error bars in figures represent the standard deviation. (a) Cycle 1, (b) Cycle 10, (c) Cycle 20, and (d) Cycle 30.

Mechanical Modeling

The data provided in this publication shows that pressure applied to a pouch cell has a significant effect on the cell's performance and degradation. This is particularly evidenced by the absence of active material cracking in the positive electrode. To better understand the distribution and magnitude of the force applied on the cathode, the clamping of the pouch cell was simulated in COMSOL Multiphysics using the Solid Mechanics module. A 3D geometry of the pouch cell and clamping plates were generated in COMSOL, the schematic of the cross-section is shown in **Figure S3**.

Since the compression setup and the pouch cell have two axes of symmetry (YZ and ZX), the simulated geometry was reduced to one quarter of its form to reduce computational expenses. The solved dataset was later mirrored to show the results for the full geometry. The boundary conditions considered for the 3D model are shown in **Figure S4** below, with the center of the bottom clamping plate fixed and simply supported in the Z direction. The circular section on the top clamping plate represents contact with the load cell in the setup, since all the applied force is transferred through it to the cell. The total applied force simulated was a quarter of the actual force to account for the reduced geometry due to symmetry.

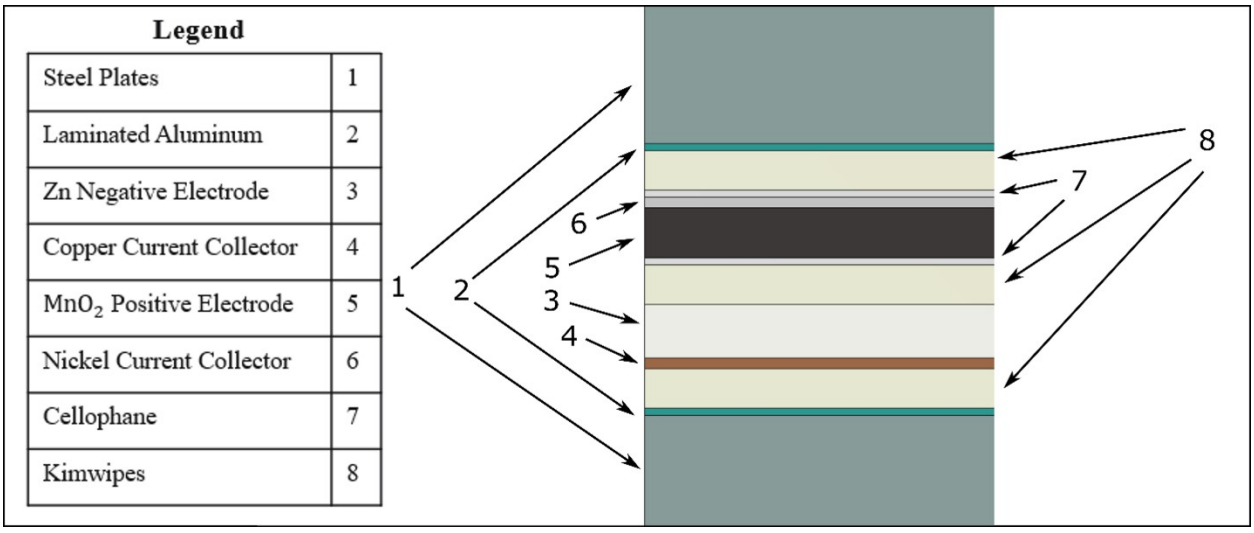

Figure S3: Schematic of clamping plates and Zn-MnO_2 pouch cell cross-section used in 3D simulation.

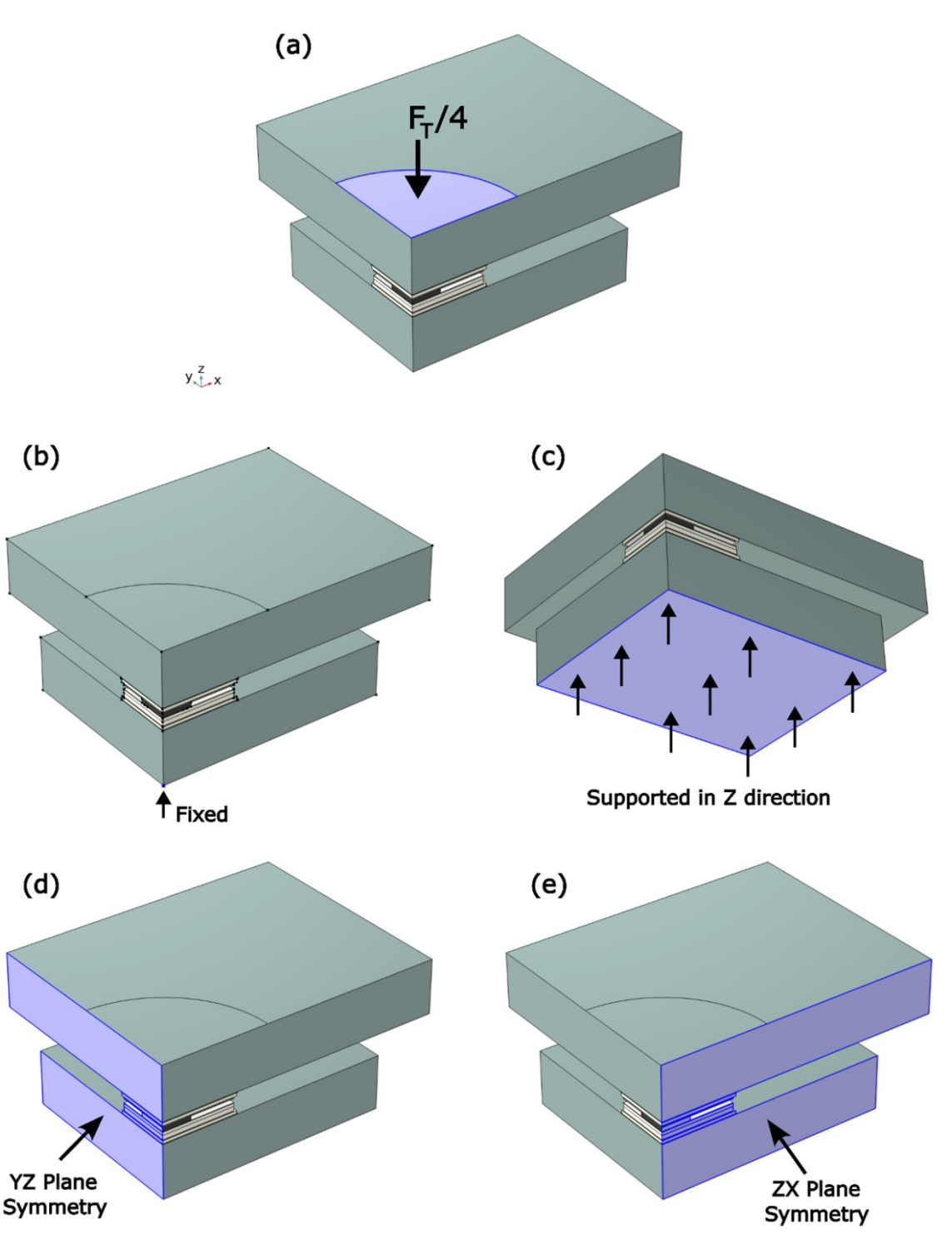

Figure S4: 3D model of the clamping plates and pouch cell, reduced to one quarter of geometry due to symmetry. Boundary conditions shown are (a) total applied load to the top plate, (b) fixed constraint at the center of the bottom plate, (c) support in Z direction for the bottom plate, (d) YZ plane symmetry, and (e) ZX plane symmetry.

All materials in the simulation were considered to be linear elastic. The clamping plates were assigned to the properties of the steel material from the COMSOL materials library. The pouch material was laminated aluminum, and was simplified to be aluminum, which was assigned the properties of aluminum from the materials library as well. The material properties for copper and nickel meshes, as well as cellophane, were found on their respective manufacturer websites [1, 2] and in the literature [3, 4].

The mechanical properties for the positive and negative electrodes were calculated using the Mori-Tanaka homogenization scheme [5]. The volume fractions of components were determined from using the weight fractions specified in the experimental section, densities of the components, and the electrodes' volume and mass data. The mechanical properties of each component were found in literature and used with volume fractions to estimate realistic Young's Moduli and Poisson's Ratios for the electrodes. A similar process was used to estimate the mechanical properties of Kimwipes using those of cellulose fibers and 50% porosity, as no properties could be found from manufacturers or in the literature. All the mechanical properties used for the materials are given below in **Table S1**.

Table S1: Mechanical properties for materials used in mechanical analysis. Calculated values for MnO_2 and Zn electrodes were determined using volume fractions and the Mori-Tanaka composite material homogenization scheme. Estimated values for the cellophane and Kimwipes were determined using the Mori-Tanaka composite material homogenization scheme with an assumed porosity of 50%.

Material	**Young's Modulus (GPa)**	**Poisson's Ratio**	**Source**
Steel	200	0.30	COMSOL Library
Aluminum	70	0.33	COMSOL Library
MnO_2 positive electrode	1.035	0.167	Calculated [5]
Zn negative electrode	3.305	0.238	Calculated [5]
Copper mesh	110	0.34	Reference [1]
Nickel mesh	200	0.31	Reference [2]
Cellophane	2.82	0.43	References [3, 4]
Kimwipe	4.03	0.20	Calculated [5]

Since the mechanical properties of various components are estimates, there is a moderate degree of uncertainty in the precise values of the quantitative results. This uncertainty does not have an impact on the qualitative results, such as the contact pressure distribution on the cathode surface.

The simulated contact pressures on the surface of the positive electrode due to 5N and 212N of total applied load are shown in **Figure S5a** and **S5b**, respectively. The pressure distribution is uniform, as evidenced by the color gradient. The pressure distribution at 212N is shown with a narrower pressure range in **Figure S5c**, along with areas of the electrode which were identified to be under a constant contact pressure of 2.00 MPa with various amounts of variance. Specifically, areas for 2.00 ± 0.04 MPa (2% variance), 2.00 ± 0.10 MPa (5% variance), and 2.00 ± 0.20 MPa (10% variance) are outlined in white.

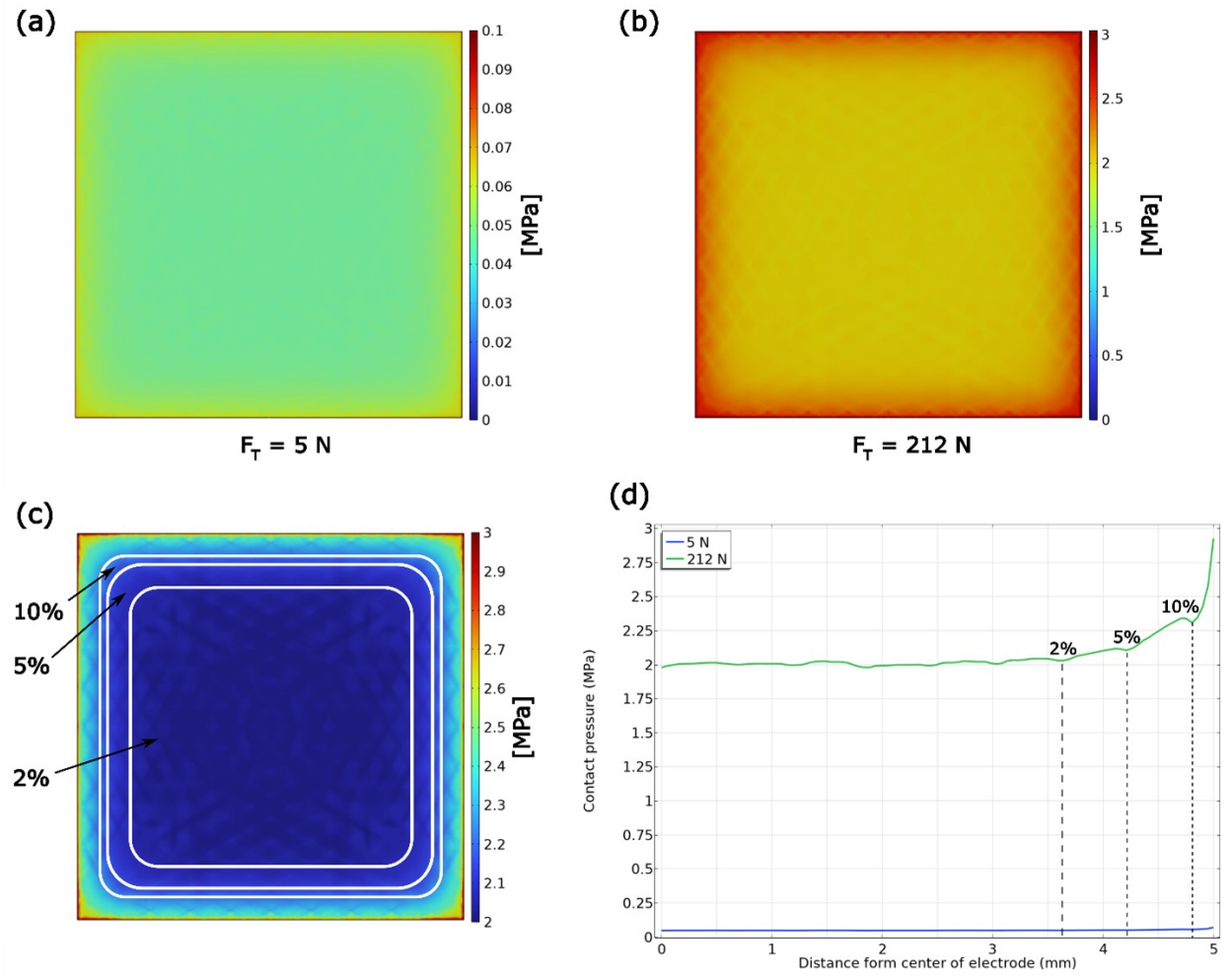

Figure S5: Simulation results showing contact pressure at the surface of the 1 cm^2 MnO_2 electrode at an applied load (F_T) of (a) 5 N and (b) 212 N. The contact pressure plot at 212 N with a narrow color range is shown in (c) where surface areas of uniform pressure +/- 2%, 5%, and 10% variance are depicted as white squares with fillets. A line plot of contact pressure in (d) spans the middle of the electrode from the center (x = y = 0) to the outer edge (y = 0, x = 5 mm).

The contact pressure of the electrode, spanning the middle of the electrode from its center (y=0, x=0) to the right edge (y=0, x=5 mm), is shown in **Figure S5d**. This plot further shows the uniformity of the contact pressure, with the magnitude of pressure significantly increasing only near the edges. The different levels of variance in pressure uniformity mentioned previously are identified by vertical dashed lines. The percentage of the surface area within each variance percentage is provided in **Table S2** below.

Table S2: Calculated pressure and simulated uniform pressure values (MPa) for the 1 cm^2 MnO_2 electrode and percent surface area for 2%, 5%, and 10% variance in pressure uniformity.

Total Applied Force, F_T (N)	**Calculated Pressure on Full Electrode (MPa)**	**Simulated Contact Pressure on Full Electrode (MPa)**	**Uniform Pressure Area, ± 2% (cm^2)**	**Uniform Pressure Area, ± 5% (cm^2)**	**Uniform Pressure Area, ± 10% (cm^2)**
212	2.12	2.00	0.522	0.700	0.777

The simulation results show that the calculated applied pressure of 2.12 MPa is a close estimate of the actual pressure the positive electrode experienced during the study. These results confirm that a large portion of the electrode should cycle as intended and support the findings from various characterization techniques used to determine that the cell benefited from the applied pressure. The simulation results are also useful for identifying areas which were subjected to higher pressure than intended (*e.g.*, the electrode edges), which may cycle in an unexpected manner.

Electrochemical Impedance Spectroscopy

Electrochemical Impedance Spectroscopy (EIS) measurements were taken by applying 5 mV sinusoidal AC amplitude from open-circuit potential at 20 kHz-0.1 Hz frequency range. The data from Nyquist plots was fitted using an equivalent circuit with ZFit software inbuilt in the battery cycler (VMP3, Biologic). The fitted results from Nyquist plots for alkaline Zn-$Mn^{O}{}_2$batteries cycled under two different externally applied pressures, *i.e.*, 0.05 MPa or 2.12 MPa are shown in **Table S3**. We observed that the externally applied pressure has profound impact on charge transfer resistance at the electrode-electrolyte interface. However, externally applied pressure has minimal impact on other parameters of equivalent circuits as shown in **Table S3.**

Table S3: Fitting results for each component of an equivalent circuit used for alkaline Zn-Mn^{O_2} batteries cycled under two different pressures.

Pressure (MPa)	Cycles	Bulk resistance (R1 in Ω)	Charge transfer resistance (R2 in Ω)	Surface film resistance (R3 in Ω)	CPE (Q1) (in F.s^(a-1)) ($\times 10^{-3}$)	a_1	Warburg element (S_2 in Ω. $s^{-1/2}$)	CPE (Q3) (in F.s^(a-1)) ($\times 10^{-3}$)	a_3
0.05	0	0.32	7.46	15.28	1.45	0.58	2.98	2.12	0.80
	20	0.50	13.24	10.23	1.62	0.79	3.40	2.94	0.76
	40	0.60	58.73	25.28	2.78	0.80	2.96	3.21	0.68
	50	0.59	62.08	19.53	2.98	0.81	3.16	3.70	0.70
2.12	0	0.43	5.36	10.60	3.75	0.65	1.89	3.14	0.80
	20	0.42	4.03	17.40	3.26	0.68	3.21	3.12	0.67
	40	0.43	4.92	18.30	2.85	0.70	2.40	3.71	0.72
	50	0.67	7.98	14.86	2.79	0.70	3.28	2.58	0.71

Energy-Dispersive X-ray Spectroscopy

Energy-Dispersive X-ray Spectroscopy (EDS) spectrum were collected using Oxford instruments X-MAX 50 mm^2 detector at an accelerating voltage of 20 kV. EDS mapping was conducted on the surface of positive electrodes cycled at 0.05 MPa and 2.12 MPa pressure and the corresponding map spectrum were recorded with the scan size of 500μm. The map spectrum collected from five different locations on the surface of each positive electrode is shown in **Figure S6**. The average concentration of Zn from five different locations on the surface of positive electrode cycled at 0.05 MPa is higher as compared to 2.12 MPa pressure **(Table S4)**. Similarly, **Figure S7** shows the EDS map spectrum collected from cross-section of Zn negative electrodes cycled at 0.05 MPa and 2.12 MPa pressures. Cross sectional EDS map spectrum shows the higher concentration of oxygen to Zn ratio for a cell cycled at 0.05 MPa. These results may indicate that the formation of ZnO is likely to be more on the surface of negative electrodes cycled at 0.05 MPa than that of electrodes cycled at 2.12 MPa pressure.

Table S4: Average concentration of Zn present on the surface of positive electrodes cycled at 0.05 MPa and 2.12 MPa pressure.

Pressure (MPa)	Concentration of Zn	
	Average (wt%)	Error
0.05	11.88	0.79
2.12	10.70	0.54

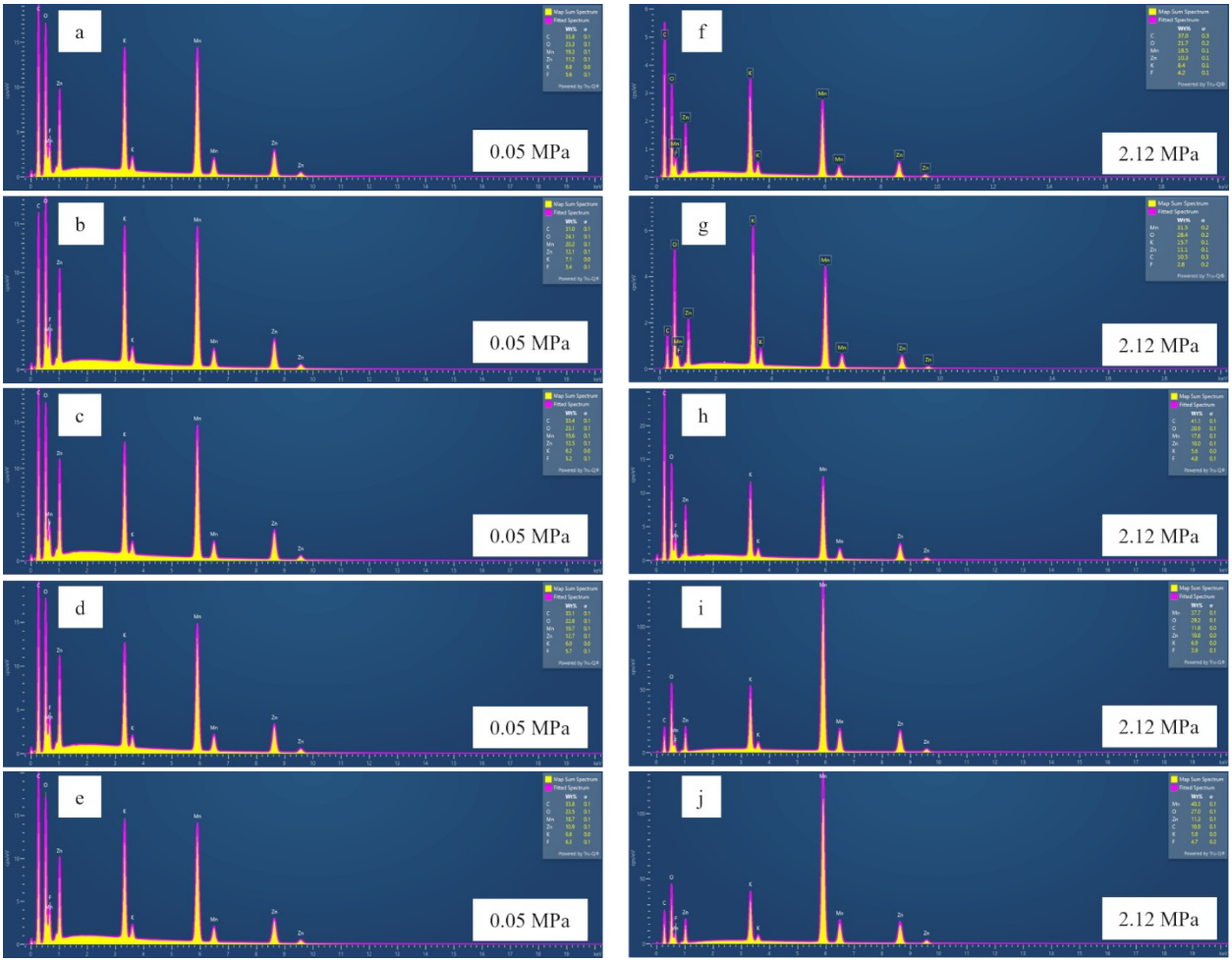

Figure S6: EDS map spectrum at five different locations on the surface of positive electrodes cycled (a-e) at 0.05 MPa pressure and (f-j) at 2.12 MPa pressure.

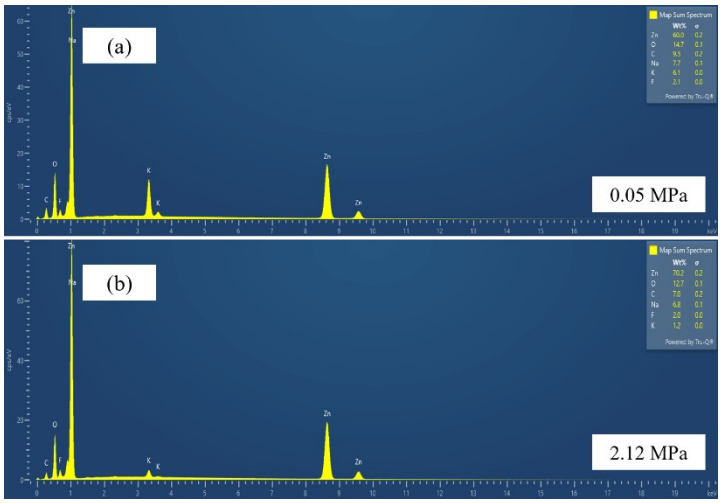

Figure S7: Cross-sectional EDS map spectrum of negative electrodes cycled (a) at 0.05 MPa pressure and (b) at 2.12 MPa pressure.

Crystal Structure

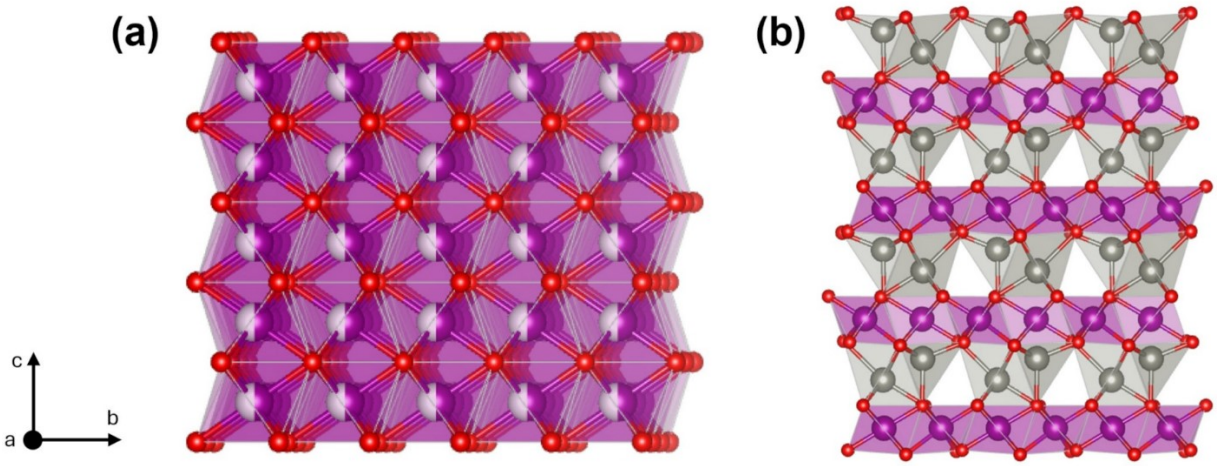

Figure S8: Crystal structures of (a) ε-MnO_2 and (b) $Zn_2Mn_3O_8$. Manganese is purple, zinc is gray, and oxygen is red.

X-ray Diffraction

Table S5: Rietveld refinement results for the XRD pattern collected on a positive electrode cycled under 0.05 MPa.

	ε-MnO_2	$Zn_2Mn_3O_8$	Graphite
Space Group	*P6₃/mmc*	*Pmn2₁*	*P6₃/mmc*
a (Å)	2.860(7)	5.96(2)	2.459(5)
b (Å)		5.02(1)	
c (Å)	4.589(8)	9.34(3)	6.711(3)
α, β, γ (°)	90, 90, 120	90, 90, 90	90, 90, 120
Crystallite Size (nm)	13(2)	8(1)	>180
Weight %	28(3)	30(4)	41(4)
$\%R_{wp}$	8.4 ($R_{f,\varepsilon\text{-}MnO2}$=10.6, $R_{f,Zn2Mn3O8}$=12.3, $R_{f,Gr}$=7.7)		

Table S6: Rietveld refinement results for the XRD pattern collected on a positive electrode cycled under 2.12 MPa.

	ε-MnO_2	$Zn_2Mn_3O_8$	Graphite
Space Group	*P6₃/mmc*	*Pmn2₁*	*P6₃/mmc*
a (Å)	2.862(8)	6.00(2)	2.472(4)
b (Å)		4.98(1)	
c (Å)	4.614(9)	9.34(2)	6.709(2)
α, β, γ (°)	90, 90, 120	90, 90, 90	90, 90, 120

Crystallite Size (nm)	14(2)	8.5(9)	>180
Weight %	22(2)	35(3)	44(4)
$\%R_{wp}$	10.3 ($R_{f,\varepsilon\text{-}MnO2}$=8.1, $R_{f,Zn2Mn3O8}$=9.4, $R_{f,Gr}$=4.3)		

Table S7: Rietveld refinement results for the XRD pattern collected on a negative electrode cycled under 0.05 MPa.

	ZnO
Space Group	*P6₃mc*
a (Å)	3.2477(4)
b (Å)	
c (Å)	5.2058(3)
α, β, γ (°)	90, 90, 120
Crystallite Size (nm)	65.8(8)
$\%R_{wp}$	22.6 ($R_{f,ZnO}$=6.9)

Table S8: Rietveld refinement results for the XRD pattern collected on a negative electrode cycled under 2.12 MPa.

	ZnO
Space Group	*P6₃mc*
a (Å)	3.2491(3)
b (Å)	
c (Å)	5.2075(2)
α, β, γ (°)	90, 90, 120
Crystallite Size (nm)	95(1)
$\%R_{wp}$	22.8 ($R_{f,ZnO}$=6.6)

References

1. Copper Mesh, *AMERICAN ELEMENTS, Americanelements.com.* 2025; Available from: https://www.americanelements.com/copper-mesh-7440-50-8.
2. Nickel Mesh, *AMERICAN ELEMENTS, Americanelements.com.* 2025; Available from: https://www.americanelements.com/nickel-mesh-7440-02-0.
3. Leppänen, I., et al., *Enzymatic Degradation and Pilot-Scale Composting of Cellulose-Based Films with Different Chemical Structures.* Journal of Polymers and the Environment, 2020. **28**(2): p. 458-470.
4. Chakraborty, I. and H. Kano, *Characterization of cellophane birefringence due to uniaxial strain by focused surface plasmon microscopy.* OSA Continuum, 2021. **4**(2): p. 409-415.
5. Mori, T. and K. Tanaka, *Average stress in matrix and average elastic energy of materials with misfitting inclusions.* Acta Metallurgica, 1973. **21**(5): p. 571-574.